Qutrit Randomized Benchmarking

A. Morvan,[1,2,*] V. V. Ramasesh,[1] M. S. Blok,[1,3] J. M. Kreikebaum,[1,4] K. O'Brien,[5] L. Chen,[1] B. K. Mitchell,[1] R. K. Naik,[1] D. I. Santiago,[1,2] and I. Siddiqi[1,2,4]

[1]*Quantum Nanoelectronics Laboratory, Department of Physics, University of California at Berkeley, Berkeley, California 94720, USA*
[2]*Computational Research Division, Lawrence Berkeley National Lab, Berkeley, California 94720, USA*
[3]*Department of Physics and Astronomy, University of Rochester, Rochester, New York 14627, USA*
[4]*Materials Sciences Division, Lawrence Berkeley National Lab, Berkeley, California 94720, USA*
[5]*Department of Electrical Engineering and Computer Science, Massachusetts Institute of Technology, Cambridge, Massachusetts 02139, USA*

(Received 20 August 2020; accepted 27 April 2021; published 27 May 2021)

Ternary quantum processors offer significant potential computational advantages over conventional qubit technologies, leveraging the encoding and processing of quantum information in qutrits (three-level systems). To evaluate and compare the performance of such emerging quantum hardware it is essential to have robust benchmarking methods suitable for a higher-dimensional Hilbert space. We demonstrate extensions of industry standard randomized benchmarking (RB) protocols, developed and used extensively for qubits, suitable for ternary quantum logic. Using a superconducting five-qutrit processor, we find an average single-qutrit process infidelity of 3.8×10^{-3}. Through interleaved RB, we characterize a few relevant gates, and employ simultaneous RB to fully characterize crosstalk errors. Finally, we apply cycle benchmarking to a two-qutrit CSUM gate and obtain a two-qutrit process fidelity of 0.85. Our results present and demonstrate RB-based tools to characterize the performance of a qutrit processor, and a general approach to diagnose control errors in future qudit hardware.

DOI: 10.1103/PhysRevLett.126.210504

Introduction.—While the majority of contemporary quantum processors encode and process information in quantum two-level systems (qubits), processors based on d-level *qudits* ($d > 2$) could both (i) store exponentially greater information and (ii) implement certain algorithms using fewer entangling gates than their qubit-based counterparts [1–4]. Recently, diverse experimental platforms including optical photons, nitrogen-vacancy centers, trapped ions, and superconducting circuits have begun to explore qudit-based information processing [5–14].

In particular, systems based on three-level qutrits are attracting growing interest. Qutrit-based processors can enable, in theory, error correction with small code size [15,16], high-fidelity magic state distillation [17], and robust quantum cryptography [18,19] and communication [20] protocols. Experimentally, single qutrits have both enabled fundamental tests of quantum mechanics [21] and been used as auxiliary systems to aid various tasks like implementing Toffoli gate [22] or multiqubit controlled-phase gates [23]. Multiqutrit algorithms have also been executed recently, both with a measurement-based photonic platforms [8,9] and a superconducting five-qutrit processor [11]. This increase in qutrit processors highlights a clear need for qutrit-ready quantum characterization, verification, and validation (QCVV) techniques.

Randomized benchmarking [24,25] (RB) is a prominent family of QCVV tools. In standard RB, a limited set of randomly chosen gate sequences is run on a quantum processor to characterize the average gate fidelity independent of state-preparation-and-measurement (SPAM) errors. Building on standard RB, interleaved and cycle benchmarking [26] variants characterize individual gates. While RB is routinely used to measure qubit gate fidelities, corresponding protocols generalizing RB to qutrits have not been demonstrated experimentally [27].

In this Letter, we develop explicit qutrit-capable recipes for both randomized benchmarking and cycle benchmarking, and experimentally demonstrate their viability on a superconducting quantum processor. Specifically, we report the use of (i) standard RB to measure average gate fidelity over single-qutrit Clifford gates, (ii) interleaved RB to measure the fidelity of individual single-qutrit gates, (iii) simultaneous RB on several qutrits to characterize and mitigate crosstalk, and (iv) cycle benchmarking to characterize a two-qutrit entangling gate. On our processor, measured single-qutrit process infidelities are on the order of 3.8×10^{-3} for an isolated qutrit. Our two-qutrit entangling gate, the controlled SUM, achieves a process fidelity of 0.85.

Processor and gate set.—Our quantum processor, detailed in Ref. [11], comprises five superconducting transmon circuits. We operate these as qutrits, encoding information in the lowest three energy levels $\{|0\rangle, |1\rangle, |2\rangle\}$. Our elementary single-qutrit gate set

consists of rotations in both the $\{|0\rangle, |1\rangle\}$, and $\{|1\rangle, |2\rangle\}$ subspaces. These subspaces can be selectively addressed with resonant microwave pulses. Additionally, we can add phases to any state using virtual gates [28] defined in software. These pulses are calibrated like qubit pulses with the difference of an added phase correction on the idle state during the pulse in order to correct the error induced by the ac-stark shift (see Supplemental Material [29] for details). Our two-qutrit gate is a controlled-SUM gate, the qutrit analog of the CNOT gate [2]. Dispersive measurement allows us to resolve, in a single shot, the $|0\rangle$-, $|1\rangle$-, and $|2\rangle$-state occupancies.

Single-qutrit randomized benchmarking.—RB relies on randomly generated sequences of gates, sampled from the Clifford group, to effectively depolarize gate errors. To implement qutrit RB, one thus needs to sample gates from the *single-qutrit* Clifford group [37]. The d-dimensional Clifford, defined as the normalizer of the Pauli group of corresponding dimension, is generated by the Hadamard gate H and phase gate S. For qutrits, with $d = 3$, these gates are defined as follows:

$$H = \frac{1}{\sqrt{3}} \begin{pmatrix} 1 & 1 & 1 \\ 1 & \omega & \omega^2 \\ 1 & \omega^2 & \omega \end{pmatrix}, \qquad S = \begin{pmatrix} 1 & 0 & 0 \\ 0 & 1 & 0 \\ 0 & 0 & \omega \end{pmatrix}, \tag{1}$$

where ω is the primitive dth root of unity. Modulo a global phase, the d-dimensional Clifford group contains $d^3(d^2-1)$ unitary operations; the single-qutrit Clifford group thus has 216 gates. Using combinations of our native applied in sequence, we generate each Clifford gate using a generalization of the so-called $ZXZXZ$ decomposition for qubits [28]—see the Supplemental Material [29] for details. On average, this decomposition requires 3.325 native gates (not including software-defined phase gates) per Clifford. Other hardware platforms, with different native gates, will necessarily use different decompositions; in principle, any gateset capable of generating both H and S can generate the full Clifford group.

We first implement the basic qutrit RB protocol, generating random Clifford sequences of depth up to 400 (with a final inversion pulse) and applying them to a single qutrit. The results are shown in Fig. 1, with Fig. 1(a) displaying the decay of basis-state populations to their steady-state value; importantly, the populations of all states decay to $1/3$, as expected for a fully depolarized state. This is a signature of Clifford twirling; using the qubit Clifford group would not fully depolarize the qutrit—see Supplemental Material [29]. This depolarization is also illustrated in Fig. 1(b), which shows the exponential decay of the expectation value of the Pauli Z operator as a function of gate depth m. The decay constant p, characterizing this evolution is related to the average process infidelity—or Pauli error—per Clifford operation e_F via

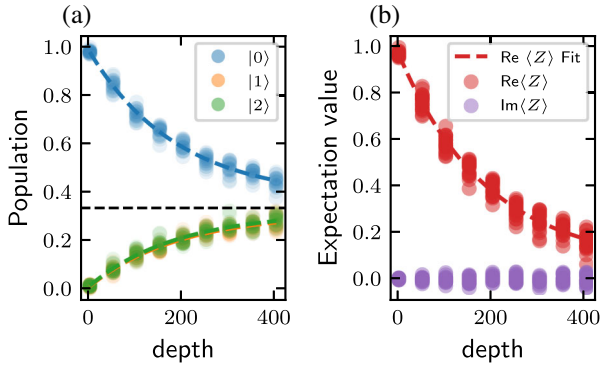

FIG. 1. Randomized benchmarking of a single qutrit. For depths up to 400, we generate 20 Clifford-random gate sequences (with a final inversion gate) and measure (a) the resulting Z-basis state occupancies and (b) the observable $\langle Z \rangle$. Each measurement is repeated 1024 times. Individual points correspond to each of the 20 randomizations, with dashed lines showing fits to a single exponential decay. As qutrit Clifford twirling effectively maps gate errors into a depolarizing channel, for long sequences the populations all tend to $1/3$ and the sequence-averaged qutrit state tends to the maximally mixed state $\rho = \frac{1}{3}\mathbb{1}_3$. Panel (b) illustrates the utility of measuring the expectation value of the Pauli operator Z and taking its real part. The imaginary part of the expectation value remains at zero throughout, which means that the RB sequence is effectively depolarizing the noise.

the relation $e_F = (1-p)(1-1/d^2)$. A couple technical points: (i) the superconducting processor we use allows for measuring $\langle Z \rangle$ with a single circuit, since all state occupancies $P(|i\rangle)$ can be measured at once, which determine $\langle Z \rangle$,

$$\langle Z \rangle = P(|0\rangle) + \omega P(|1\rangle) + \omega^2 P(|2\rangle), \tag{2}$$

(ii) while the Pauli Z operator is not Hermitian, the phase of $\langle Z \rangle$ does not change under depolarization; thus the imaginary component, which by preparation was zero initially, remains zero throughout.

Table I shows the average process infidelities for single-qutrit Clifford gates on each of the our processor's qutrits, extracted via qutrit RB. These errors, on the order of 5×10^{-3}, are higher than those associated with single-qubit pulses.

Understanding single-qutrit error sources.—To understand the sources of error in our single-qutrit gates, we begin by separating these into incoherent errors and coherent errors. In the Supplemental Material [29] we estimate the contribution of known coherent errors, including pulse errors leading to over- or underrotations or ac Stark shifts, and find that are likely not dominant. Here we present a simple model to estimate the error from decoherence during the gate operation.

Our model of decoherence in a three-level transmon includes five total processes: two decay processes ($|2\rangle \to |1\rangle$ and $|1\rangle \to |0\rangle$) and three dephasing processes

(in the $|0\rangle/|1\rangle$, $|1\rangle/|2\rangle$, and $|0\rangle/|2\rangle$ subspaces). This ladder structure notably ignores parity-suppressed direct decay from the second-excited state $|2\rangle$ to the ground state $|0\rangle$, consistent with experiments [38]. We denote the rates of the decay processes by $\Gamma_{21} = 1/T_1^{(21)}$ and $\Gamma_{10} = 1/T_1^{(10)}$, and those of the dephasing processes by $\Gamma_2 = 1/T_2^{(01)}$, $\Gamma_3 = 1/T_2^{(12)}$, and $\Gamma_4 = 1/T_2^{(02)}$. Here $T_1^{(10)}$ and $T_2^{(01)}$ correspond to the usual T_1 and T_2 parameters used to describe qubit decoherence. Under this decay model, the time evolution of the density matrix $\rho(t)$ in the absence of external drives is given (in terms of the initial elements ρ_{ij}) by

$$\rho(t) = \begin{pmatrix} 1-\rho_{11}e^{-\Gamma_{10}t} - \frac{\rho_{22}}{\Gamma_{10}-\Gamma_{21}}\left(\Gamma_{10}e^{-\Gamma_{21}t} - \Gamma_{21}e^{-\Gamma_{10}t}\right) & \rho_{01}e^{-\Gamma_2 t} & \rho_{02}e^{-\Gamma_3 t} \\ \rho_{10}e^{-\Gamma_2 t} & \rho_{11}e^{-\Gamma_{10}t} + \rho_{22}\frac{\Gamma_{21}}{\Gamma_{10}-\Gamma_{21}}\left(e^{-\Gamma_{21}t} - e^{-\Gamma_{10}t}\right) & \rho_{12}e^{-\Gamma_4 t} \\ \rho_{20}e^{-\Gamma_3 t} & \rho_{21}e^{-\Gamma_4 t} & \rho_{22}e^{-\Gamma_{21}t} \end{pmatrix}. \quad (3)$$

As shown in the Supplemental Material [29], this model agrees well with measured dynamics of the transmon on our processor. Each decay rate in the model is directly measurable; values for qutrits on our processor are shown in Table I. Using this model, one can calculate the theoretical process-infidelity limit $e_F^{(c)}$ for a process of duration τ. In the limit of short pulses ($\tau \ll T_1, T_2$), this limit is directly proportional to the duration

$$e_F^{(c)} \simeq \frac{1}{9}(2\Gamma_2 + 2\Gamma_3 + 2\Gamma_4 + \Gamma_{10} + \Gamma_{21})\tau. \quad (4)$$

Table I reports the coherence limit for our single-qutrit pulses of duration $\tau = 3.325 \times (30 + 2)$ ns, where 30 ns is the duration of a native pulse and 2 ns the delay between two consecutive pulses. We use dephasing times measured from echo experiment as it gives a better estimate for the RB procedure: RB sequence can present dynamical decoupling behavior that decouples from low frequency noise, like TLS, for instance, that are known to reduce the dephasing time measured with Ramsey experiment. The values reported in the table are averaged over one month of measurements. As the table shows, the calculated coherence-limited process infidelities are within the error bar of the experimentally measured values, corroborating our initial estimate that errors from decoherence are dominant over coherent errors. This implies that the quality of achievable single-qutrit transmon gates will increase along with improvements in coherence times. Theoretically, one could try to achieve better fidelity with shorter gates; however, we found that the amplitude needed made crosstalk cancellation impossible.

TABLE I. Coherence times and single qutrit process infidelity measured for our 5 qutrits. Coherence times are defined in the main text. Specific of the measurement is given in the Supplemental Material [29]. The coherences are the average of several measurement over the period of the experiment. The error indicated in parenthesis indicates the uncertainty on the last digits by reporting the standard deviation of these measurements. $e_F^{(c)}$ indicates the coherence limit of the process error calculated with Eq. (4).

Quantity	Unit	Q_1	Q_2	Q_3	Q_4	Q_5
$T_1^{(10)}$	(μs)	53(7)	60(10)	45(23)	53(3)	57(4)
$T_1^{(21)}$	(μs)	27(5)	36(3)	28(4)	26(3)	34(5)
$T_2^{(01)}$	(μs)	50(20)	60(10)	49(26)	52(21)	56(13)
$T_2^{(12)}$	(μs)	20(5)	27(7)	20(11)	24(8)	26(8)
$T_2^{(02)}$	(μs)	24(8)	36(11)	34(14)	31(9)	35(7)
$e_F^{(c)}$	$\times 10^{-3}$	3.3(9)	2.5(6)	3.0(1.3)	2.9(8)	2.6(6)
e_F	$\times 10^{-3}$	4.7(2)	2.8(2)	3.3(3)	4.4(7)	4.0(2)

We now discuss two variations of single-qutrit randomized benchmarking interleaved and simultaneous RB, before moving on to benchmarking two-qutrit gates.

Interleaved randomized benchmarking.—As with qubits, the basic standard RB protocol measures gate error averaged over the set of Clifford gates. Interleaved RB (IRB) enables the characterization of specific gates, allowing, for example, to measure the contribution of each subspace rotation. In interleaved RB, one interleaves the gate of interest between the Clifford twirls. While any gate can, in principle, be characterized by IRB, practically it is helpful if the interleaved gate is itself a Clifford gate as this makes the final inversion gate easy to calculate. Comparing the decay constants measured with and without interleaving, one can get an estimate of the error associated with the interleaved gate itself.

In our case, we demonstrate the use of IRB to characterize both elementary gates, comprising a single pulse from our native gate set, as well as a composite gate. The elementary gates we characterize are rotations by π about the X axis in both the $\{|0\rangle, |1\rangle\}$ and $\{|1\rangle, |2\rangle\}$ subspaces. These elementary gates are naturally elements of the single-qutrit Clifford group and are thus easily characterized using IRB. The composite gate we characterize is the qutrit Hadamard gate, useful in many algorithms (e.g., quantum Fourier transform). With our native gates, a Hadamard requires four microwave pulses.

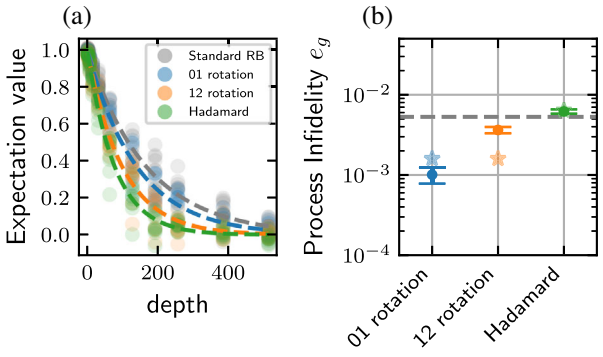

FIG. 2. Interleaved RB of three single-qutrit gates: (i) π rotation in the $\{|0\rangle, |1\rangle\}$ subspace (blue), (ii) π rotation in the $\{|0\rangle, |1\rangle\}$ subspace (orange), and (iii) the qutrit Hadamard gate H. (a) Depolarization decay for standard (no interleaving) qutrit RB (gray) as a reference, and interleaved sequences for each of the three gates under test. As in Fig. 1, each point represents a single random sequence measured 1024 times. (b) Process infidelities (dots) of each gate calculated from the data in (a). Also plotted for comparison (stars) is an estimation of the process infidelity from the Clifford-averaged value computed in the previous section: Our decomposition used an average of 3.325 native gates per Clifford, so a simple estimate for gate error for an n-pulse gate is $n/3.325$ times the Clifford average. For a Hadamard, $n = 4$; for the π rotations, $n = 1$.

Figure 2 shows the decay curves obtained for our native π rotations gate, and the Hadamard gate, using interleaved RB. The estimation of the gate error is given by [39]

$$e_{\text{gate}} = \left(1 - \frac{1}{d^2}\right)\left(1 - \frac{p_i}{p}\right), \tag{5}$$

where p_i and p are the decay probabilities with and without interleaving, respectively. For the π pulses, we find errors around 1×10^{-3} in the $\{|0\rangle, |1\rangle\}$ subspace and around 4×10^{-3} in the $\{|1\rangle, |2\rangle\}$ subspace. Though both subspace rotations have the same duration, their error rate is significantly different. For the composite Hadamard gate, we report a process infidelity of $e_H = (6.2 \pm 0.4) \times 10^{-3}$, competitive with other implementations of this gate [40]. This infidelity is close to what one would expect from a simple scaling of the average Clifford error e_F by the ratio of durations of the Hadamard gate to the average Clifford duration. These results emphasize that the infidelity measured by randomized benchmarking is an average over all the Cliffords, which here are composites gates, but the gate set basis can have different errors measurable through IRB.

Crosstalk.—Another important application of RB is to measure the addressability, or single-qudit gate crosstalk, on a given device [37]. Usually, crosstalk errors are characterized with a simultaneous RB experiment where two (or more) qudits undergo a RB sequence at the same time. Transmon qutrits are more sensitive to crosstalk than qubits, as the use of the second level increases the frequency crowding. A significant challenge in the use of a transmon-based device as a qutrit processor is to mitigate these unwanted effects [11]. Simultaneous qutrit RB enables quantifying this crosstalk. Figure 3 shows the results of simultaneous RB with and without crosstalk cancellation developed in Ref. [11]. This mitigation technique is designed to cancel fields incident on other qutrits when driving a targeted qutrit that results from microwave crosstalk present in the device. Figure 3 makes apparent the significant improvement on the crosstalk from such a procedure. Notably, the gain is not homogeneous over the whole chip. In the Supplemental Material [29], we give results for more than 2 qutrits.

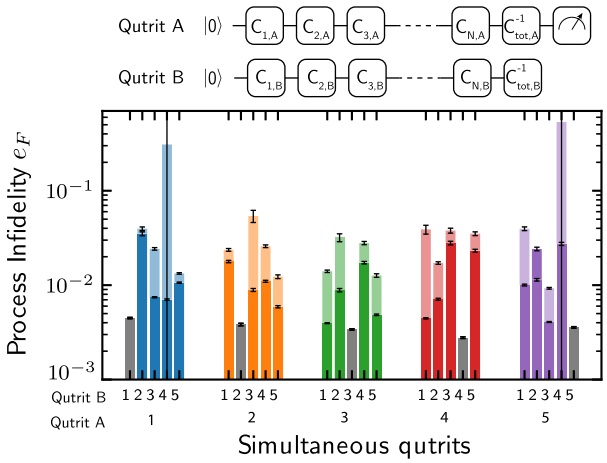

FIG. 3. Average error per Clifford while simultaneously running RB sequences on two qutrits. The solid bars indicate the average error per Clifford with the crosstalk cancellation applied to the system; transparent bars are corresponding errors without cancellation. The gray bars indicate isolated qutrit results. Note that the large uncertainties are for noncancelled crosstalk.

Cycle benchmarking for two-qutrit gates.—We now turn to characterizing two-qutrit gates. While RB is, in principle, possible here, it would require sampling from the full two-qutrit Clifford group. This is impractical both due to the size of the Clifford group (roughly 5×10^6 elements) and due to the fact that the vast majority of these gates require multiple elementary entangling gates to implement. To circumvent these problems and properly characterize two-qutrit entangling gates, we instead generalize the recently demonstrated cycle benchmarking technique [26].

Like interleaved RB, cycle benchmarking (CB) sandwiches the gate under test between randomly chosen gates; in CB, however, these random gates are sampled from the Pauli rather than Clifford group. A key advantage of this Pauli twirling is that two-qudit Pauli gates are simply tensor products of one-qudit Pauli gates, and thus do not require entangling gates. Unlike Clifford twirling, however, Pauli twirling does not fully depolarize the gate noise; instead, it maps all errors into stochastic Pauli errors. Normally, this would result in population survival curves which, unlike

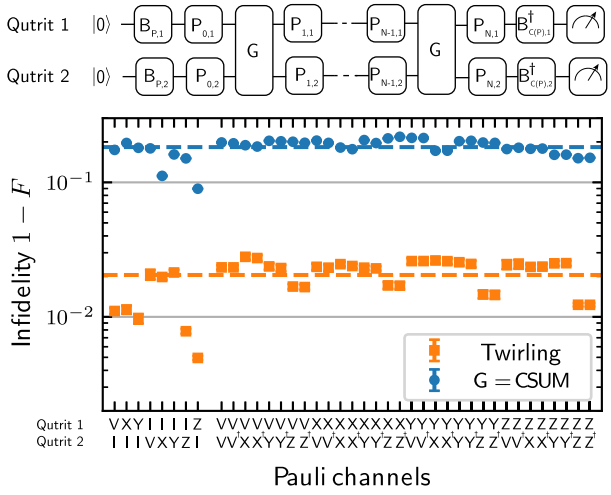

FIG. 4. Cycle benchmarking of the entangling controlled-SUM (CSUM) gate. For comparison, we have included the same experiment with (orange) only Pauli twirling, i.e., using no interleaved gate (for a control), and (blue) with the interleaved CSUM. We present the exponential decay obtained for each Pauli channel (we have omitted the complex conjugate as its value is identical). The process fidelity is calculated by averaging all the Pauli channels, yielding a process infidelity of 2.22×10^{-2} for the control (or average over the 9^2 2-qutrit Pauli that compose the twirling)—and 1.83×10^{-1} for the CSUM.

RB, do not follow a single exponential decay. However, in CB, the initial state is chosen to be a Pauli eigenstate, and the final measurement basis is the Pauli basis. This recovers a single exponential decay. Averaging over the measured decay parameters for each initial state and measurement basis yields the average error per gate.

The protocol for a qutrit system is quite similar to the qubit protocol for the main twirling part: the gate of interest is interleaved in a random sequence of qutrit Pauli gates. However, differences appear in the measurement and the state preparation necessary to measure a single exponential decay at a time. The most notable difference comes from the fact that each Pauli operator commutes with its Hermitian conjugate $P^\dagger = P^2$ which is also a Pauli operator. Hence, they share the same eigenbasis and qutrit CB only uses 4 state preparation and measurement operators B_Q for a single qutrit—compared to 3 for the qubit case—leading to a total of 4^N for an N-qutrit system for the choice of the initial gate. The four basis rotations are given in the Supplemental Material [29]. Another important point arises from this observation: the expectation values of a Pauli operator and its Hermitian conjugate are complex conjugates, i.e., $\langle P^\dagger \rangle = \overline{\langle P \rangle}$ implying that the Pauli decay associated with these two operators is the same. A more detailed analysis is given in the Supplemental Material [29]. This allows us to report the decay associated with only half of all the N-Pauli channels. As these statements follow from the structure of the Pauli group, they generalize to all qudit systema.

We have applied this qutrit CB protocol without any gate (as a control) and the two-qutrit controlled-SUM gate [11]. The results are shown in Fig. 4. It is a slow gate of duration of 1.5 μs that rely on the always-on coupling between the two qutrits. We measure an average process fidelity of 0.98 for the control experiment and 0.82 for the CSUM gate. Using Eq. (5), this corresponds to a gate fidelity of 0.85.

Conclusion.—We have demonstrated the characterization of a qutrit processor by extending randomized benchmarking and cycle benchmarking to qutrits. With the protocols developed in this Letter, qutrit processors can be meaningfully compared to their qubit-based counterparts. As RB has become a workhorse in characterizing qubit processors, we anticipate that qutrit RB will see similarly widespread use. In addition to developing qutrit RB protocols, we have demonstrated the viability of qutrit processors based on transmon circuits: specifically, single-qutrit gates—both in isolation and simultaneous—achieve fidelities comparable to qubit-based devices.

The authors gratefully acknowledge the conversations and insights of D. Gottesman, J. Emerson, J. Wallman, W. Livingston, and J.-L. Ville. This work was supported by the test bed program of the Advanced Scientific Computing Research for Basic Energy Sciences program, Office of Science of the U.S. Department of Energy under Contract No. DE-AC02-05CH11231.

*amorvan@lbl.gov

[1] T. C. Ralph, K. Resch, and A. Gilchrist, Phys. Rev. A **75**, 022313 (2007).
[2] D. Gottesman, in *NASA International Conference on Quantum Computing and Quantum Communications* (Springer, New York, 1998), pp. 302–313.
[3] Z. Gedik, I. A. Silva, B. Çakmak, G. Karpat, E. L. G. Vidoto, D. d. O. Soares-Pinto, E. Deazevedo, and F. F. Fanchini, Sci. Rep. **5**, 14671 (2015).
[4] S. S. Bullock, D. P. O'Leary, and G. K. Brennen, Phys. Rev. Lett. **94**, 230502 (2005).
[5] B. P. Lanyon, T. J. Weinhold, N. K. Langford, J. L. OBrien, K. J. Resch, A. Gilchrist, and A. G. White, Phys. Rev. Lett. **100**, 060504 (2008).
[6] R. K. Naik, N. Leung, S. Chakram, P. Groszkowski, Y. Lu, N. Earnest, D. C. McKay, J. Koch, and D. I. Schuster, Nat. Commun. **8**, 1904 (2017).
[7] C. S. Wang, J. C. Curtis, B. J. Lester, Y. Zhang, Y. Y. Gao, J. Freeze, V. S. Batista, P. H. Vaccaro, I. L. Chuang, L. Frunzio *et al.*, Phys. Rev. X **10**, 021060 (2020).
[8] Y.-H. Luo, H.-S. Zhong, M. Erhard, X.-L. Wang, L.-C. Peng, M. Krenn, X. Jiang, L. Li, N.-L. Liu, C.-Y. Lu *et al.*, Phys. Rev. Lett. **123**, 070505 (2019).
[9] X.-M. Hu, C. Zhang, B.-H. Liu, Y. Cai, X.-J. Ye, Y. Guo, W.-B. Xing, C.-X. Huang, Y.-F. Huang, C.-F. Li *et al.*, Phys. Rev. Lett. **125**, 230501 (2020).

[10] P. Imany, J. A. Jaramillo-Villegas, M. S. Alshaykh, J. M. Lukens, O. D. Odele, A. J. Moore, D. E. Leaird, M. Qi, and A. M. Weiner, npj Quantum Inform. **5**, 1 (2019).
[11] M. Blok, V. Ramasesh, T. Schuster, K. OBrien, J. Kreikebaum, D. Dahlen, A. Morvan, B. Yoshida, N. Yao, and I. Siddiqi, Phys. Rev. X **11**, 021010 (2021).
[12] F. Dolde, V. Bergholm, Y. Wang, I. Jakobi, B. Naydenov, S. Pezzagna, J. Meijer, F. Jelezko, P. Neumann, T. Schulte-Herbrggen *et al.*, Nat. Commun. **5**, 3371 (2014).
[13] C. Senko, P. Richerme, J. Smith, A. Lee, I. Cohen, A. Retzker, and C. Monroe, Phys. Rev. X **5**, 021026 (2015).
[14] R. Bianchetti, S. Filipp, M. Baur, J. M. Fink, C. Lang, L. Steffen, M. Boissonneault, A. Blais, and A. Wallraff, Phys. Rev. Lett. **105**, 223601 (2010).
[15] S. Muralidharan, C.-L. Zou, L. Li, J. Wen, and L. Jiang, New J. Phys. **19**, 013026 (2017).
[16] E. T. Campbell, Phys. Rev. Lett. **113**, 230501 (2014).
[17] E. T. Campbell, H. Anwar, and D. E. Browne, Phys. Rev. X **2**, 041021 (2012).
[18] H. Bechmann-Pasquinucci and A. Peres, Phys. Rev. Lett. **85**, 3313 (2000).
[19] D. Bruß and C. Macchiavello, Phys. Rev. Lett. **88**, 127901 (2002).
[20] A. Vaziri, G. Weihs, and A. Zeilinger, Phys. Rev. Lett. **89**, 240401 (2002).
[21] R. Lapkiewicz, P. Li, C. Schaeff, N. K. Langford, S. Ramelow, M. Wieniak, and A. Zeilinger, Nature (London) **474**, 490 (2011).
[22] A. Fedorov, L. Steffen, M. Baur, M. P. da Silva, and A. Wallraff, Nature (London) **481**, 170 (2012).
[23] C. Song, S.-B. Zheng, P. Zhang, K. Xu, L. Zhang, Q. Guo, W. Liu, D. Xu, H. Deng, K. Huang *et al.*, Nat. Commun. **8**, 1061 (2017).
[24] E. Knill, D. Leibfried, R. Reichle, J. Britton, R. B. Blakestad, J. D. Jost, C. Langer, R. Ozeri, S. Seidelin, and D. J. Wineland, Phys. Rev. A **77**, 012307 (2008).
[25] E. Magesan, J. M. Gambetta, and J. Emerson, Phys. Rev. A **85**, 042311 (2012).
[26] A. Erhard, J. J. Wallman, L. Postler, M. Meth, R. Stricker, E. A. Martinez, P. Schindler, T. Monz, J. Emerson, and R. Blatt, Nat. Commun. **10**, 5347 (2019).
[27] M. Jafarzadeh, Y.-D. Wu, Y. R. Sanders, and B. C. Sanders, New J. Phys. **22**, 063014 (2020).
[28] D. C. McKay, C. J. Wood, S. Sheldon, J. M. Chow, and J. M. Gambetta, Phys. Rev. A **96**, 022330 (2017).
[29] See Supplemental Material at http://link.aps.org/supplemental/10.1103/PhysRevLett.126.210504 for derivation and extra data, which includes Refs. [30–36].
[30] J. Kreikebaum, K. OBrien, A. Morvan, and I. Siddiqi, Supercond. Sci. Technol. **33**, 06LT02 (2020).
[31] F. Arute, K. Arya, R. Babbush, D. Bacon, J. C. Bardin, R. Barends, R. Biswas, S. Boixo, F. G. S. L. Brandao, D. A. Buell *et al.*, Nature (London) **574**, 505 (2019).
[32] S. Sheldon, L. S. Bishop, E. Magesan, S. Filipp, J. M. Chow, and J. M. Gambetta, Phys. Rev. A **93**, 012301 (2016).
[33] F. Motzoi, J. M. Gambetta, P. Rebentrost, and F. K. Wilhelm, Phys. Rev. Lett. **103**, 110501 (2009).
[34] J. M. Chow, L. DiCarlo, J. M. Gambetta, F. Motzoi, L. Frunzio, S. M. Girvin, and R. J. Schoelkopf, Phys. Rev. A **82**, 040305(R) (2010).
[35] Z. Chen, J. Kelly, C. Quintana, R. Barends, B. Campbell, Y. Chen, B. Chiaro, A. Dunsworth, A. G. Fowler, E. Lucero *et al.*, Phys. Rev. Lett. **116**, 020501 (2016).
[36] P. Dita, J. Phys. A **36**, 2781 (2003).
[37] J. M. Gambetta, A. D. Córcoles, S. T. Merkel, B. R. Johnson, J. A. Smolin, J. M. Chow, C. A. Ryan, C. Rigetti, S. Poletto, T. A. Ohki *et al.*, Phys. Rev. Lett. **109**, 240504 (2012).
[38] M. J. Peterer, S. J. Bader, X. Jin, F. Yan, A. Kamal, T. J. Gudmundsen, P. J. Leek, T. P. Orlando, W. D. Oliver, and S. Gustavsson, Phys. Rev. Lett. **114**, 010501 (2015).
[39] E. Magesan, J. M. Gambetta, B. R. Johnson, C. A. Ryan, J. M. Chow, S. T. Merkel, M. P. da Silva, G. A. Keefe, M. B. Rothwell, T. A. Ohki *et al.*, Phys. Rev. Lett. **109**, 080505 (2012).
[40] M. A. Yurtalan, J. Shi, M. Kononenko, A. Lupascu, and S. Ashhab, Phys. Rev. Lett. **125**, 180504 (2020).